

DiT-HC: Enabling Efficient Training of Visual Generation Model DiT on HPC-oriented CPU Cluster

Jinxiao Zhang

Department of Earth System Science
Tsinghua University
Beijing, China
zhang-jx22@mails.tsinghua.edu.cn

Runmin Dong*

School of Artificial Intelligence
Sun Yat-sen University
Zhuhai, China
dongrm3@mail.sysu.edu.cn

Mengxuan Chen

Department of Earth System Science
Tsinghua University
Beijing, China
chenmx21@mails.tsinghua.edu.cn

Yunpu Xu

Institute of Data and Information
Tsinghua Shenzhen International
Graduate School
Shenzhen, China
xuyp25@mails.tsinghua.edu.cn

Shenggan Cheng

National University of Singapore
Singapore, Singapore
shenggan@comp.nus.edu.sg

Qinrui Zheng

National Supercomputing Center in
Shenzhen
Shenzhen, China
zhengqr@nsccsz.cn

Haohuan Fu*

Institute of Data and Information
Tsinghua Shenzhen International
Graduate School
Shenzhen, China
haohuan@tsinghua.edu.cn

Xiyong Wu

Institute of Data and Information
Tsinghua Shenzhen International
Graduate School
Shenzhen, China
wuxiyong25@mails.tsinghua.edu.cn

Yi Zhao

Department of Earth System Science
Tsinghua University
Beijing, China
zhang-y19@mails.tsinghua.edu.cn

Jianting Liu

National Supercomputing Center in
Shenzhen
Shenzhen, China
liujt@nsccsz.cn

Abstract

Generative foundation models have become an important tool for data reconstruction and simulation in scientific computing, showing a tight integration with traditional numerical simulations. At the same time, with the development of new hardware features, such as matrix acceleration units and high-bandwidth memory, CPU-based clusters offer promising opportunities to accelerate and scale such models, facilitating the unification of artificial intelligence and scientific computing. We present DiT-HC, the first system to train and scale the generative model DiT on a next-generation HPC CPU cluster. DiT-HC introduces three key techniques: (1) communication-free tensor parallelism (CFTP) with AutoMem for automated memory-aware dataflow, (2) HCOps, a suite of optimized GEMM and operator kernels leveraging vector and matrix acceleration units, and (3) a custom MPI backend that overlaps computation, communication, and memory movement. Experiments show $8.2\times$ – $87.7\times$ speedups over native or public CPU libraries and 90.6% weak scaling efficiency on 256 nodes. These results demonstrate the feasibility of large-scale generative model training on CPU clusters and provide new insights for future HPC-AI co-design.

1 Introduction

Artificial intelligence is becoming increasingly prevalent in scientific research, and scientific computing is shifting from a paradigm centered solely on numerical simulation to one where simulations and data-driven models co-develop in a complementary manner[9, 18, 35]. While this shift enhances modeling capability[4] and improves the efficiency of data utilization, it also places new demands on high-performance computing (HPC) platforms: they must not only continue to support large-scale simulations in domains such as climate and seismology, but also run generative foundation models efficiently to enable data-driven optimization in areas such as data assimilation[16, 43], parameterization schemes[5, 8], and bias correction[13, 21]. Consequently, HPC platforms are supposed to support both numerical simulation and model training to achieve a unified workflow.

HPC-oriented CPU cluster is one of the most established and widely deployed computing infrastructures in modern supercomputers, forming the backbone of large-scale numerical simulations and scientific applications. In generative model training, GPUs/TPUs are the primary platforms[24], while CPU clusters provide only limited support for efficient training of deep learning models. The primary reason for

*Corresponding Authors

this gap lies in the general-purpose nature of CPUs: their architectures emphasize versatility but typically provide lower compute density and memory bandwidth than GPUs. For deep learning workloads dominated by large-scale matrix operations and intensive memory access workloads, these limitations directly constrain training efficiency, placing CPUs at a disadvantage in scaling generative models and posing challenges unifying AI and HPC on the same platform.

Consequently, there is a trend for next-generation HPC-oriented CPU architectures to incorporate AI-focused hardware features, such as matrix acceleration units (MAUs) and on-package high-bandwidth memory (OPM), which provide new opportunities for deep learning model training. For example, the Armv9 architecture introduces two-dimensional ZA registers and the Scalable Matrix Extension (SME) instruction set, significantly improving the efficiency of matrix and tensor computations [41]. Intel’s Sapphire Rapids processors similarly integrate Advanced Matrix Extensions (AMX), enabling more efficient execution of AI workloads [22]. In addition, modern HPC CPUs are adopting hierarchical memory structures that combine on-package high-bandwidth memory with traditional DDR, alleviating the bandwidth bottlenecks of conventional designs. However, fully exploiting these new features is non-trivial: unlike the highly encapsulated GPU ecosystem with its mature toolchains, CPU platforms involve distinct characteristics in instruction set extensions, hierarchical memory management, and NUMA-domain interconnects, which necessitate systematic rethinking of operator implementations, parallelization strategies, and memory scheduling.

In this context, we select the generative foundation model DiT as our case study to investigate efficient training and scalable optimization on HPC-oriented CPU clusters. On the one hand, diffusion models have become the dominant paradigm in visual content generation [15, 26, 27, 29, 32, 36, 37], and Transformer-based DiT [10, 28] serves as a representative with strong global modeling capacity and scalability. On the other hand, diffusion models have also demonstrated significant value in scientific domains [20], achieving advances in satellite image super-resolution [6], multimodal image fusion [3], ensemble weather forecasting [30], and Earth system data assimilation [14, 16, 38]. Therefore, DiT combines the representativeness of cutting-edge generative models with practical relevance in scientific applications, making it a representative target for evaluating and optimizing next-generation CPUs in large-scale training.

In this paper, we introduce DiT-HC, a scalable high performance training framework for DiT on a new HPC-oriented CPU cluster, the LS pilot system with LX2 CPUs. DiT-HC is elaborately designed to exploit the hierarchical memory and matrix acceleration hardware of LX2, enabling scalable and high-throughput training. We validate DiT-HC using remote sensing datasets and show its cross-domain transferability,

and high parallel efficiency. Experimental results show DiT-HC achieves a 8.2 \times performance improvement over the native high-performance software stack and achieves 90.6% weak scaling efficiency when scaling to 256 nodes.

Our main contributions are summarized as follows:

1. We optimized DiT training on a HPC-oriented CPU cluster, improving efficiency and scalability, and validated its correctness and transferability on remote sensing data.
2. We propose a communication-free tensor parallelism method named CFTP and present an automatic memory dataflow management module AutoMem to fully utilize the hierarchical OPM-DDR memory structure.
3. We release an extended PyTorch operator math library named HCOps, which includes optimized matrix tiling schemes for GEMM and low-level intrinsic optimizations for AI operators to better exploit the vector and matrix acceleration units.
4. To reduce resource contention, we implement a custom communication backend supporting MPI asynchronous collective communication and overlap computation, communication, and memory operations across different CPU cores.

2 Related Works

Several attempts have explored deep learning training on CPU-based supercomputers. The Fugaku system [7] with A64FX processors optimized oneDNN to scale applications [33], while the Sunway Taihulight system [11] employed swCaffe [25] for distributed training. CPUs have also been used for memory-intensive tasks: Huang [17] proposed hierarchical training for recommendation models, and Intel researchers [19] optimized deep recommendation workloads on Skylake/Cascade Lake CPUs. At large scale, You et al. [44] trained AlexNet in 11 minutes using 2,048 Xeon CPUs with LARS. These works demonstrate the feasibility of CPU-based training, particularly for memory-demanding workloads, but they mainly targeted non-Transformer models that are less representative in today’s large-model landscape, and their optimizations were highly case-specific rather than generalizable.

At the operator level, high-performance math libraries provide essential support. oneDNN [1] accelerates deep learning across multiple platforms, while Arm-specific efforts such as autoGEMM [42], LBBGEMM [40], and automatic micro-kernel generation [2] optimize GEMM computations through dynamic tiling, auto-tuning, or code generation. Although these methods achieve strong performance on traditional CPUs, they remain focused on vector-based instruction sets and fail to exploit newer architectural features such as matrix acceleration units (MAUs) and on-package high-bandwidth memory, limiting their effectiveness on processors like LX2.

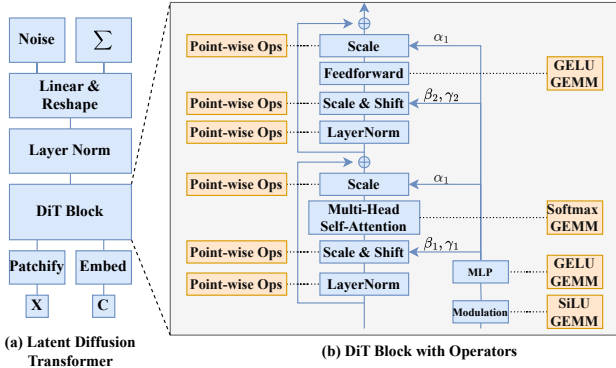


Figure 1. The workflow of DiT and corresponding operators.

At the framework level, diffusion and Transformer models have motivated specialized optimizations. DiffusionPipe [39] explored pipeline-parallel training strategies for DiT, while general Transformer frameworks such as xFormers [23], MEATTEN [12], OneFlow [45], DeepSpeed [31], and Megatron [34] introduced operator fusion, modular attention kernels, and distributed scaling methods. Among them, MEATTEN targets Arm CPUs with fusion and tiling optimizations. However, the majority of these frameworks are GPU-centric, making them difficult to port to CPU clusters. This gap highlights the need for CPU-specific frameworks that can exploit new architectural features while supporting representative Transformer-based generative models such as DiT.

3 Preliminaries and Analysis

3.1 Architecture of Diffusion Transformers

Diffusion Transformer (DiT) is a state-of-the-art visual generation framework built upon Denoising Diffusion Probabilistic Models (DDPM). By leveraging self-attention mechanisms and modular design, DiT significantly enhances the scalability of the model and the quality of generation. DiT revolutionizes noise prediction by architecting a fully transformer based network that processes latent variables through the following components.

1. *Patchify*: the input latent variable $x_t \in \mathbb{R}^{H \times W \times C}$ is divided into $N = \frac{H}{p} \times \frac{W}{p}$ patches of size $p \times p$, then linearly projected into a D -dimensional sequence.

$$z_t = \text{Linear}(\text{Flatten}(x_t)) \in \mathbb{R}^{N \times D}. \quad (1)$$

2. *Conditional Transformer Block*: each block comprises Multi-Head Self-Attention (MSA), Adaptive Layer Normalization (AdaLN) and the Feed-Forward Network (FFN). AdaLN encodes the timestep t and the class label (or other conditions) y into the modulation parameters, which can be formalized as equation 2.

$$\gamma_t, \beta_t = \text{MLP}(t), \quad \text{AdaLN}(h) = \gamma_t \odot \text{LayerNorm}(h) + \beta_t. \quad (2)$$

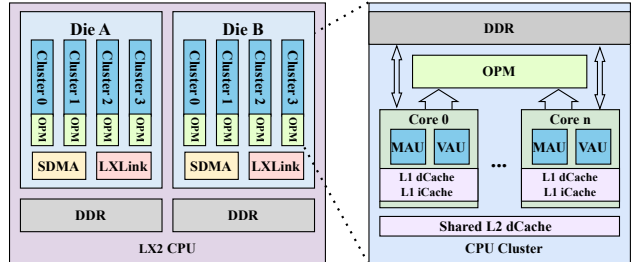


Figure 2. Architecture of the LX2 CPU.

Then the MSA models global contextual relationships based on the attention mechanism.:

$$\text{Attention}(Q, K, V) = \text{Softmax}\left(\frac{QK^\top}{\sqrt{D}}\right)V, \quad (3)$$

where $Q, K, V \in \mathbb{R}^{N \times D}$ are generated via linear transformations of the input sequence.

3. *Output Reconstruction*: the final sequence is reconstructed into the noise prediction $\epsilon_\theta(x_t, t)$ via a de-patchify layer.

We have outlined the specific operators involved in the DiT model structure, as illustrated in Figure 1. During the entire training process, the computational workload is primarily dominated by matrix multiplication kernels (aten::matmul or aten::addmm operators and their corresponding backward processes). Additionally, several commonly used AI operators, such as activation functions (e.g., Gelu, Silu, and Softmax), normalization operations (e.g., LayerNorm), and various mathematical operations (e.g., tanh, scale, and addition), also contribute to the overall computational load.

3.2 Overall Architecture of LX2 CPU

This work is based on the 256-node cluster named LS pilot system. Each node is equipped with two LX2 high-performance CPUs having more than 256 cores. The LX2 CPU is a system on a chip integrating two computing Dies in the package. Each Die is equipped with 128GB off-die DDR memory, along with 4 NUMA domains. Within each NUMA domain, CPU cores share the on-package memory (OPM) and the L2 cache. In order to improve the data movement efficiency between DDR and OPM, System Direct Memory Access (SDMA) interface is implemented in each CPU Die. Dies are also interconnected through an LXLink network, with each network card providing a bidirectional bandwidth of 48 GB/s. In each core, it supports vector and matrix computation based on the vector acceleration units (VAU) and matrix acceleration unit (MAU), with double-precision floating-point SIMD instructions and 8×8 matrix computation within the pipeline. The cores operate at a frequency over 1.3GHz.

3.3 Hierarchical OPM-DDR Hybrid Memory

3.3.1 **Limited memory capacity.** In the hierarchical OPM-DDR hybrid memory architecture, the first factor to consider

is the memory capacity. While OPM offers excellent bandwidth performance, its capacity is relatively limited, much smaller than that of DDR memory. Furthermore, each CPU cluster is equipped with only 32GB of DDR space, which presents a significant challenge for deep learning training. Current deep learning models typically require tens of gigabytes of memory to store model parameters and training states, making it difficult to scale the model’s batch size, thus limiting hardware efficiency during the training process. As the model size increases, insufficient memory not only affects training efficiency but may also lead to memory overflow, further exacerbating the bottleneck in hardware resources.

3.3.2 Memory access performance. Memory access performance is another critical consideration. The bandwidth of OPM is independent between CPU clusters following the NUMA architecture, which means that remote OPM access across CPU clusters significantly increases latency and reduces bandwidth. Specifically, remote OPM access within the same Die results in about a 50% decrease in bandwidth compared to its original value; when accessing across Dies within the same CPU, the bandwidth drops to 37%; and for inter-CPU access within the same node, the bandwidth is reduced to only 10% of the original value. In contrast, DDR bandwidth is shared within a Die. Although each CPU cluster in the NUMA architecture has its own DDR private space, experimental results show that local and remote DDR access within the same Die exhibit similar performance. When accessing remote DDR across Dies within the same CPU, performance drops to 75% of its original value, and when accessed across CPUs within the same node, the performance decreases to 37%, similar to the performance loss observed with remote OPM access.

These performance results suggest that in designing an efficient memory access strategy, it is crucial to minimize remote OPM access across NUMA nodes and DDR access across Dies to avoid performance bottlenecks caused by bandwidth loss. On the other hand, the consistent DDR access performance within a Die offers great opportunity for resource management across NUMA nodes.

3.4 Matrix Acceleration Units

The Matrix Acceleration Unit (MAU) in the LX2 CPU supports double-precision 8x8 matrix computation within the pipeline, offering powerful computational capabilities. Maximizing the utilization of the MAU is crucial for performance in deep learning applications. The key factor that determines whether the MAU can deliver optimal performance is whether data can be fed into the vector registers promptly, enabling better pipeline throughput for the MAU. To figure out this issue, we conducted a series of profiling tests and identified several important factors that affect the efficiency of MAU-based GEMM computations. First, L2 cache utilization plays a critical role—when memory access patterns that

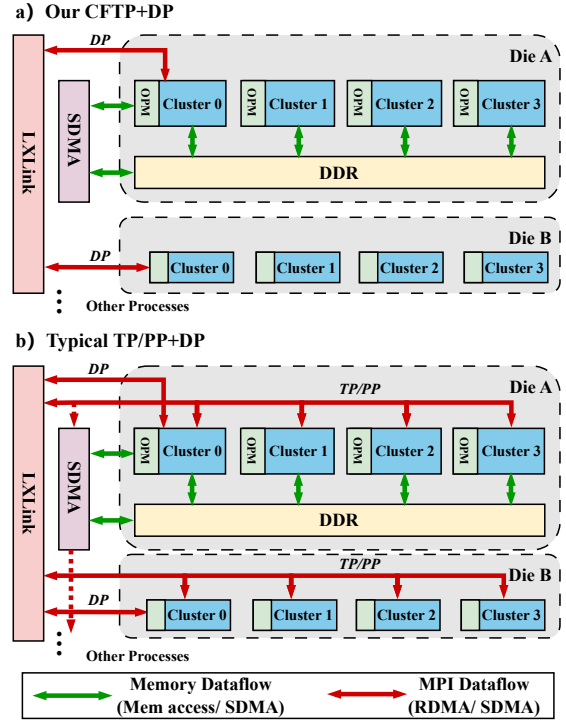


Figure 3. Communication dataflow comparison between typical TP/PP and our CFTP.

are more L2 cache-friendly are used to supply data for matrix computations, MAU utilization improves. Second, the TLB miss ratio is another influential factor. We found that using huge page memory significantly reduces the TLB miss ratio, which in turn enhances MAU utilization, benefiting both OPM and DDR memory. Lastly, memory bandwidth also impacts performance; when matrix data resides in OPM, computation efficiency is higher than when the data is located in DDR.

To improve MAU utilization, it is essential to adopt memory access patterns that are friendly to L2 cache and to ensure that matrix data is primarily stored in OPM huge page memory. However, these requirements make manual data flow management complex and may result in application code that is difficult to maintain and reuse. Therefore, it is necessary to explore automated methods for efficiently managing data flow across hybrid memory.

4 Design and Implementations

4.1 Parallel Strategy: CFTP with DP

4.1.1 Data Parallel. Due to the significant efficiency loss when accessing remote OPM and DDR across Dies, we allocate the computational resources of a single Die to each DP process, rather than using a larger resource range. For DP implementation, we follow the standard PyTorch DDP approach, with each die storing a full replica of the model.

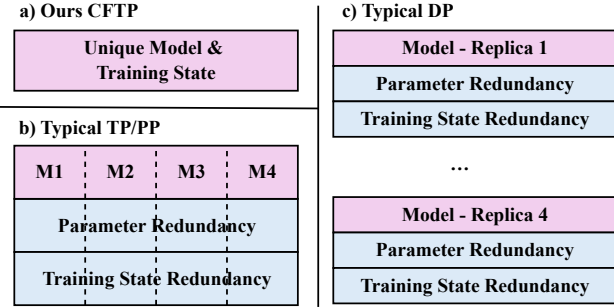


Figure 4. Memory usage comparison for a Die between typical TP/PP, DP and our CFTP.

4.1.2 CFTP: Communication-Free Tensor Parallel. As analyzed in Section 3.3, CPU clusters within a die share the same DDR controller, and DDR access—whether local or remote within the die—exhibits consistent latency and bandwidth. Moreover, DDR bandwidth is substantially higher than that of the LXLink interconnect. Based on these observations, we enable synchronization and sharing among TP nodes via direct memory operations instead of MPI processes. This eliminates the communication overhead of conventional TP methods and allows TP nodes to reside in the same process space, reducing both communication and memory redundancy during model scaling.

Figure 3 compares the communication overhead of different die-level parallelism methods. In Figure 3(a), our method assigns one process per die, with TP implemented across CPU clusters within the die. Training requires MPI only for gradient reduction across dies, resulting in just four MPI processes per compute node. By contrast, Figure 3(b) shows typical TP or PP implementations. These approaches require not only gradient synchronization between DPs but also synchronization or activation transfers within each node. While SDMA can reduce LXLink traffic, it introduces contention with DDR-OPM transfers, degrading memory performance. Unlike MPI in-place operations, SDMA also requires additional memory buffers to ensure reliability, causing extra memory overhead and frequent allocations. Consequently, typical TP/PP schemes increase the MPI process count to 16 per node, complicating the overlap of memory and communication flows and hindering balanced hardware utilization.

For memory usage within a single die (Figure 4), our method in Figure 4(a) manages all memory within one process, enabling flexible partitioning of any tensor (inputs, weights, gradients, activations) during matrix computations. This eliminates the need to exchange intermediate results, making CPU clusters fully independent and requiring only a single copy of the model and training state. By contrast, typical TP/PP methods increase memory consumption due to cross-process partitioning. TP requires partitioning to be fixed at initialization, usually limited to weights, leading to

Algorithm 1: Our AutoMem_Module Wrapper

```

1 Class AutoMem_Module(nn.Module):
2     Ori_Module = nn.Module;
3     def forward( $X_i$ ):
4         pre_forward():
5             Barrier checking whether  $X_i, W_i$  has been
6             loaded;
7             Prefetch  $W_{i+1}$ ;
8             Register post_backward() hook on
9                  $W_i.\text{acc\_grad}$ ;
10            set MemType(OPM-HugePage);
11             $X_{i+1} \leftarrow \text{Ori\_Module}.\text{forward}(X_i, W_i)$ ;
12            post_forward():
13                Offload  $X_i, W_i$ ;
14                Register pre_backward() hook on  $X_{i+1}$ ;
15                set MemType(DDR);
16
17            def backward( $dX_{i+1}$ ):
18                pre_backward():
19                    Barrier checking  $dX_{i+1}, X_i, W_i$ ;
20                    Prefetch  $W_{i-1}, X_{i-1}$ ;
21                    set MemType(OPM-HugePage);
22                     $dX_i, dW_i \leftarrow \text{Ori\_Module}.\text{backward}()$ ;
23                post_backward():
24                    Offload  $W_i, X_i, dW_i$ ;
25                    set MemType(DDR);
26
27            def train():
28                warmup_forward():
29                    Record execution order of Modules;
30                    Initialize_MemPool();
31                    Activation_Reference_track();
32                    AutoMem_Module.forward();
33                    ...

```

broadcast or aggregation of inputs and activations. PP caches intermediate activations between stages, with memory usage growing alongside pipeline depth, and may introduce load imbalance across clusters. Similarly, DP stores full model replicas on each device, which results in high memory redundancy and becomes a bottleneck to batch size scalability as device count grows.

In summary, the combined use of CFTP and DP significantly alleviates communication and memory bottlenecks under hierarchical memory architectures.

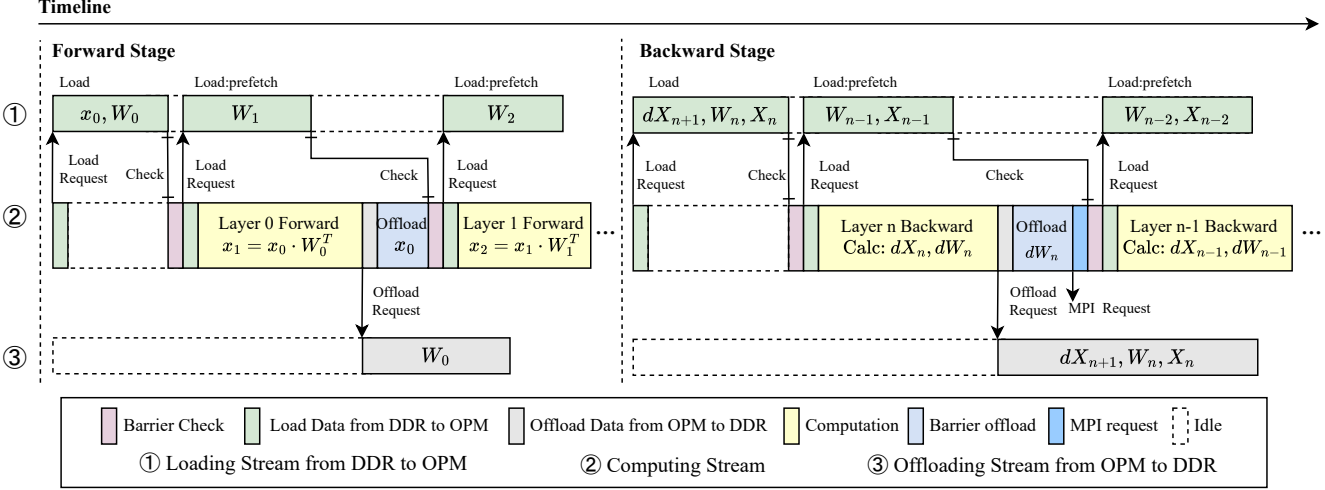


Figure 5. Overlapped dataflow based on our AutoMem. Different stream are distributed to different CPU cores.

4.2 AutoMem: Automatic Memory Dataflow Management Module

Optimizing the performance of HPC-oriented CPUs with OPM-DDR hierarchical memory requires fine-grained management of dataflow across memory levels. Manual strategies are complex and hard to generalize; therefore, we design AutoMem, a non-intrusive automated memory management module for deep learning training. AutoMem improves utilization of high-bandwidth on-package memory (OPM), enhances operator efficiency, and accelerates end-to-end DLT training—all without modifying model-level code—while ensuring that optimization strategies remain reusable for future workloads.

Algorithm 1 outlines the implementation of AutoMem. The original `nn.Module` is wrapped by `AutoMem_Module`, with `pre_forward()` invoked before the forward pass and `post_forward()` after it. In `pre_forward()`, AutoMem checks whether inputs and weights X_i, W_i reside on OPM; if not, they are loaded. It also prefetches the next layer’s weights W_{i+1} . A `post_backward()` hook is registered on the `AccumulateGrad` object of W_i , triggered once gradients are accumulated. Memory allocation is temporarily switched to OPM HugePages to ensure forward-context data remain on OPM. The forward computation then produces X_{i+1} . In `post_forward()`, X_i and W_i are offloaded back to DDR, and a hook is set on X_{i+1} to trigger its gradient loading. Finally, allocation defaults back to DDR to avoid overusing OPM HugePages.

The backward process follows a conceptually similar design, with `pre_backward()` and `post_backward()` hooks. `pre_backward()` ensures required tensors (dX_{i+1}, W_i, X_i) are loaded into OPM and prefetches W_{i-1} and X_i for the next backward step. Memory allocation mode is switched to OPM HugePages, then the original backward pass produces dX_i and dW_i . In `post_backward()`, W_i and X_i are offloaded to

DDR and allocation is reset. This completes one forward and backward cycle.

During training initialization, AutoMem performs a warm-up forward pass to record module dependencies and enable prefetching. It then initializes a pinned DDR HugePage memory pool to ensure sufficient and stable bandwidth for offloading operations. This lightweight pinned memory pool, integrated as a core component of AutoMem, provides efficient support for memory transfers. In addition, AutoMem tracks the reference relationships of inputs and activations at the memory level during the warm-up stage to determine when they can be safely offloaded during training.

All load and offload operations are implemented with SDMA and managed by dedicated CPU cores (Figure 5). Stream 2 serves as the main computation flow, occupying nearly the entire die. In contrast, Streams 1 and 3 are dedicated to data transfers, each using only one independent CPU cores. At the beginning of forward and backward passes, the first layer blocks until data are loaded into OPM; afterwards, AutoMem overlaps asynchronous prefetching and offloading with computation. For gradient tensors requiring global communication, blocking offloading is performed on the main computation cores to ensure correctness, as indicated by the blue blocks in Figure 5. This design achieves efficient overlap of computation and memory operations while incurring minimal additional core overhead via independent SDMA devices.

4.3 Operator-Level Optimization

To improve the utilization of the Matrix Acceleration Unit (MAU) and Vector Acceleration Unit (VAU), we optimized computationally intensive components of the model, including GEMM and commonly used AI operators. For GEMM,

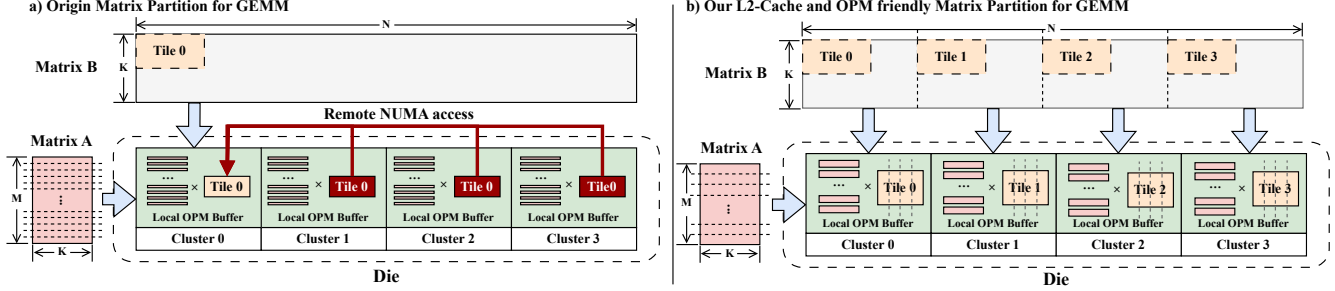


Figure 6. The diagram of our optimized GEMM with L2 Cache and memory access-friendly tiling strategy.

we redesigned the tiling strategy to increase L2 cache efficiency and balance thread workloads. In addition, we optimized operators such as GeLU, SiLU, LayerNorm, Softmax, and FlashAttention. Finally, building on these operator-level improvements, we introduced system-level tuning strategies—including parallel partitioning, NUMA-aware data transfer, and multi-level buffering—to further enhance scalability. Together, these optimizations are integrated into the HCOps extension package, enhancing both the PyTorch framework and the native software stack.

4.3.1 GEMM: numa and L2 cache friendly matrix tiling. We adopt the vendor-provided BLAS library in the native software stack, referred to as nativeBLAS, as the baseline for GEMM computations. NativeBLAS employs a closed-source kernel with instruction reordering and tiling, where matrix B is shared and matrix A is partitioned along the M -dimension. Specifically, the main thread loads a tile of B into the local OPM buffer, performs packing to ensure memory access continuity, and then shares the tile with all threads. Each thread i loads its assigned sub-matrix A_i into a private buffer, multiplies it with B_{Tile} , and writes the result to C_i .

This design, however, suffers from two key drawbacks. First, except for the NUMA node where the main thread resides, other clusters must fetch B_{Tile} from remote OPM, which introduces high latency. Second, within each cluster, a large number of cores simultaneously access different memory addresses of matrix A . These accesses converge on the shared L2 cache, creating severe contention. As a result, the effective L2 cache hit ratio drops significantly, preventing data reuse and ultimately constraining the computational throughput of the MAU.

To address these issues, we propose a NUMA- and cache-aware 2D partitioning scheme (Figure 6(b)). At the outer level, matrix B is divided along the N -dimension into sub-matrices assigned to CPU clusters (e.g., four partitions for four clusters). Each cluster independently computes $A \times B_{cid}$, with its tiles packed into local OPM buffers and retained in the L2 cache using loop unrolling. At the inner level, A_{Tile} is partitioned into m segments along M and B_{Tile} into n segments along N , resulting in $m \times n$ subtasks distributed

evenly across threads. Compared with nativeBLAS, which partitions A_{Tile} into m_{native} segments, our approach reduces the partition count to m ($m < m_{\text{native}}$), thereby improving cache reuse. This significantly increases L2 cache utilization and enhances the computational efficiency of the MAU.

4.3.2 Optimization of AI operators. Beyond GEMM, we optimized several key operators on LX2 to exploit the VAU and MAU more effectively, including GeLU, SiLU, Softmax, LayerNorm, FlashAttention, and fundamental mathematical kernels. For example, as for Tanh-GELU, a hybrid approximation scheme accelerates forward and backward passes by $13.3\times$ and $12.9\times$ with negligible loss of accuracy. For the AdamW optimizer, an operator-fusion design reduces memory writes and achieves a $12.5\times$ iteration speedup. In addition, recompilation strategies for FlashAttention and fused multiply-add kernels reduce memory residency and overall memory demand. These optimizations, integrated into HCOps, complement the GEMM improvements and contribute to end-to-end performance gains.

4.3.3 Scalability-oriented Tuning. To further address scalability bottlenecks introduced by multi-core execution and hierarchical memory, we performed systematic tuning of GEMM parallelization and synchronization strategies. The optimizations combined NUMA-aware data transfer, asynchronous inter-core communication, packing, double/triple buffering for memory and registers, tiling, and thread reuse. By exploring parameter combinations across these techniques, we identified the best-performing implementation, which forms the Tuned version of our framework and delivers the highest single-node performance.

4.4 Asynchronous Communication Backends

We implement a customized MPI-based backend to address the limitations of PyTorch’s native MPI backend and to achieve improved overlap between communication and computation. The native backend does not support asynchronous collectives such as MPI_Iallreduce. Moreover, the worker threads responsible for communication are created only after PyTorch DDP initialization and are managed uniformly

by PyTorch’s native OpenMP runtime. As a result, communication requests and computation tasks are scheduled on the same cores, forcing frequent context switches between computation and communication. This degrades both communication throughput and computational efficiency. In addition, communication and computation tasks each introduce their own synchronization mechanisms. When executed on the same cores, the contention for hardware resources further exacerbates performance loss. By customizing the MPI backend, we enable the use of asynchronous communication interfaces and allow explicit binding of communication and computation tasks to different CPU cores. This design reduces resource contention and achieves more effective overlap between communication and computation.

5 Experiments

5.1 Setting Details

Hardware and Software. All optimizations in this study are conducted on the LX2 CPU hardware architecture within the LS Pilot System, which consists of 256 nodes (detailed in Section 3.2). The software environment is based on the OpenEuler 22.03 operating system, with Clang 17.0.0 as the compiler and OpenMPI for communication. For mathematical and deep learning acceleration libraries, a combined baseline of nativeBLAS optimized for the LX2 CPU together with oneDNN 3.6.2 is employed. The model implementation and optimizations are developed on PyTorch 2.5.1. To ensure the correctness of results, additional validation experiments are performed on the NVIDIA H100 SXM5 GPUs equipped with 80 GB of HBM3 memory.

Model and Dataset The proposed DiT-HC architecture is evaluated across multiple model scales, including DiT-S/2, DiT-B/2, DiT-L/2, and DiT-XL/2, to demonstrate the effectiveness of our optimizations under different model sizes and kernel configurations. Training settings follow the original DiT implementation, employing the AdamW optimizer with a base learning rate of 10^{-4} .

Experimental evaluation involves three complementary datasets representing different modalities: the general-purpose ImageNet dataset, and two remote sensing datasets derived from Gaofen-2 and Sentinel-2 satellites. The Gaofen-2 dataset provides 4-band multispectral imagery at spatial resolution of 2m/pixel, while the Sentinel-2 dataset contains 13-band multispectral imagery at a spatial resolution of 10m/pixel.

Evaluation. Training is performed with the Mean Squared Error (MSE) loss between predicted and target latents, enforcing pixel-level reconstruction fidelity for both training from scratch and fine-tuning. For final evaluation, we adopt the Fréchet Inception Distance (FID) to assess the perceptual realism of generated images. FID is computed as the 2-Wasserstein distance between the feature distributions of real and generated images, where the mean vector and covariance matrix are estimated from features extracted using

Table 1. FID (\downarrow is better) results on remote sensing datasets, where $bs = 112$ compares GPU and LX2; $bs = 28,672$ shows effectiveness.

Dataset	GPU (112)	LX2 (112)	LX2 (28,672)
Gaofen-2	30.44	28.51	24.70
Sentinel-2	24.97	29.03	22.61

a pretrained Inception-v3 network. Lower FID values indicate that the generated distribution is closer to the real data distribution.

5.2 Accuracy Validation

To verify the correctness of our optimized training methods, we designed two types of experiments: an early-stage training scenario, where the model is trained from scratch on ImageNet, and a late-stage training scenario, where a well-converged pretrained model is fine-tuned on new remote sensing datasets.

In the training-from-scratch experiments, we conduct 1,000 training steps under two batch-size settings: a single-node batch size of 112 and the largest global batch size in our experiments, 28672. This design serves two purposes: validating the consistency of results between the LX2 CPU cluster and the NVIDIA H100 GPU. In the training-from-scratch stage, we ran DiT-XL/2 on ImageNet for 1,000 steps with two batch-size settings: a single-node batch size of 112 and the largest global batch size in our experiments, 28,672. This setup verifies the consistency of results between the LX2 CPU cluster and the NVIDIA H100 GPU, and demonstrate that even at the largest training scale, the model can still converge effectively. In Figure 7, different colors denote the per-step loss values obtained on different platforms and batch-size settings. The two dashed lines show smoothed versions of the oscillating loss curves, providing a clearer view of the convergence trend.

In the fine-tuning stage, the pretrained model was adapted to the Gaofen-2 and Sentinel-2 datasets for 1,000 steps using two batch-size settings: 112 and 28,672. For each configuration, 10,000 images were generated and compared with 10,000 real samples from the corresponding dataset to compute the Fréchet Inception Distance (FID). Table 1 summarizes the results: with a batch size of 112, the proposed optimized training method enables stable DiT training on LX2 while maintaining generation quality comparable to the NVIDIA H100. With a batch size of 28,672, the results demonstrate that the model can continue learning effectively even under extremely large-scale training. Figure 8 presents visual examples produced by the fine-tuned DiT-HC model, further confirming the reliability of our framework and its ability to generalize across different domains of scientific data.

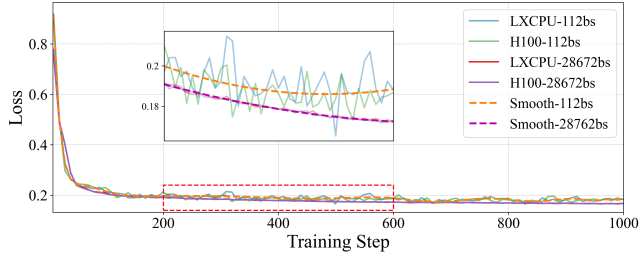


Figure 7. Comparison of loss curve of pretraining on ImageNet.



Figure 8. Visual results of the original pretrained model and finetuned model on Gaofen-2 by our DiT-HC.

Table 2. Comparison of single-step execution time and peak memory consumption across different strategies.

Batch Size	Model Size	Iteration Time (s)			Peak Memory (GB)		
		DP+TP	DP	CFTP	DP+TP	DP	CFTP
112	XL/2	-	-	13.18	-	-	358
	L/2	-	23.31	9.92	-	474	304
	B/2	8.7	6.55	3.97	309	247	198
	S/2	3.91	2.11	2.48	224	182	167
224	XL/2	-	-	29.15	-	-	346
	L/2	-	-	22.88	-	-	290
	B/2	17.89	11.45	9.75	270	277	186
	S/2	6.3	3.56	3.83	287	197	180

-: Out Of Memory

5.3 Results for Different Model Size

We conduct experiments on DiT models of varying scales, including DiT-S/2, DiT-B/2, DiT-L/2, and DiT-XL/2. The results under different parallel strategies with two global batch sizes are summarized in Table 2. For the **DP+TP** configuration, the input data is replicated across clusters within each TP group. In the **DP** setting, each cluster stores a complete copy of the model parameters, gradients, and optimizer states. Both strategies can cause large models to exceed memory capacity. In terms of peak memory usage, **CFTP** achieves the lowest consumption among all tested cases. We also observe that **DP** yields shorter iteration times for smaller models. This is because DP avoids model partitioning by maintaining full copies of the parameters, thereby improving GEMM

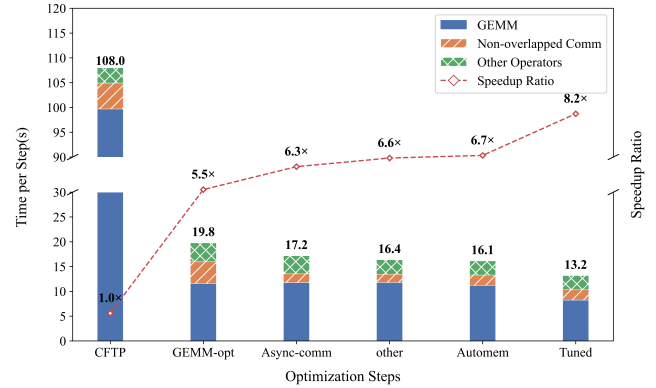


Figure 9. Stepwise optimization evaluation of our proposed methods.

efficiency at the expense of memory usage. Although the **DP+TP** strategy reduces memory consumption by grouping four clusters into a single TP group, it still incurs unavoidable intra-die communication overhead. In contrast, our proposed **CFTP** eliminates die-level communication among clusters introduced by TP, thereby achieving higher efficiency than **DP+TP**. Experimental results across all four model scales confirm the effectiveness and general applicability of this strategy.

5.4 Stepwise Results

To evaluate the optimizations proposed in Section 4, we perform stepwise ablation experiments. The baseline training framework is PyTorch compiled with NativeBLAS as the math library, oneDNN as the deep learning acceleration library, and MPI as the communication backend. As discussed in Section 4.1.2, **CFTP** is included in the baseline to mitigate memory footprint issues.

Building on this baseline, we first introduce GEMM optimization, which raises the speedup to 5.5×. Compared with NativeBLAS, the optimized GEMM reduces cross-NUMA memory access and improves L2 cache hit rates through cache-friendly task partitioning. We then incorporate an asynchronous communication backend; by assigning communication tasks to dedicated cores, the speedup further increases to 6.3×. Adding AI operator optimizations brings an additional improvement, raising the speedup to 6.6×. On top of this, integrating AutoMem—which analyzes the computation graph and prefetches data for both forward and backward passes—slightly improves the performance to 6.7×. Finally, by applying tuning strategies targeting multi-core parallelism and hierarchical memory, including NUMA-aware partitioning, multi-level buffering for memory and registers, and parameter combination optimizations, the single-node speedup ultimately reaches 8.2×.

5.5 GEMM Optimization

In DiT training, matrix multiplication constitutes the dominant computational workload, making GEMM optimization a decisive factor for overall performance. In this section, we examine the performance of GEMM operators and compare our implementations against OpenBLAS, NativeBLAS, and oneDNN across different DiT model sizes. As shown in Table 3, OpenBLAS provides unsatisfactory performance due to the lack of architecture-specific optimizations for the new processors. Although NativeBLAS and oneDNN are the default libraries, they are not NUMA-aware at the Die level and exhibit low cache hit rates.

To address these issues, we first design our GEMM kernels that maximize data locality and avoid cross-NUMA memory accesses. As shown in Table 4, these kernels achieve up to $35.49\times$ speedup over NativeBLAS at the module level. Building on this foundation, we further introduce our Tuned kernels, which apply a set of refined strategies including NUMA-aware task partitioning, multi-level buffering for memory and registers, and parameter tuning for multi-core parallelism. With these enhancements, our Tuned version achieves even higher performance, further extending the gains obtained by our GEMM kernels.

Table 3. Single-step training time (in seconds) of DiT models using OpenBLAS, NativeBLAS, oneDNN, our GEMM kernels, and our Tuned version. Our GEMM provides a substantial reduction in iteration time compared with standard libraries, while our Tuned version further improves performance through multi-core and memory hierarchy optimizations.

Model Size	Iteration Time (s)				
	OpenBLAS	NativeBLAS	oneDNN	our GEMM	our Tuned
XL/2	1156.37	154.41	147.18	16.14	13.18
L/2	636.08	91.72	64.86	14.52	9.92
B/2	181.66	41.42	19.82	5.83	3.97
S/2	47.90	22.35	8.96	4.02	2.48

Table 4. Speedup of our optimized GEMM in latency of the individual linear modules compared to nativeBLAS.

Name	Dimensions	Speedup (x)
qkv_proj	1152×3456	30.10
o_proj	1152×1152	13.89
up_proj	1152×4608	16.49
down_proj	4608×1152	35.49
condition_proj	1152×6912	1.73

5.6 Performance Comparison with GPU System

To position the performance of our CPU-based system relative to GPUs, we conducted a comparative experiment under comparable system-level compute capability. The GPU side consisted of two 8-GPU H100 servers, each H100 delivering 495 TFLOPS in TF32 without sparsity, while the

CPU system is built upon HPC-oriented processors whose peak floating-point capability is slightly lower than that of H100 GPUs. The two platforms differ markedly in memory and interconnect characteristics. Each H100 server provides ultra-high-bandwidth HBM, NVLink-based intra-node interconnect, and multi-rail InfiniBand for inter-node communication, whereas the CPU platform offers substantially lower aggregated memory bandwidth and inter-processor interconnect bandwidth, resulting in different communication and memory-access behaviors.

With a global batch size of 3,584, the CPU system achieves 182.47 TFLOPS sustained performance and an end-to-end training time of 13.5 s per iteration, compared to 7.6 s on the H100 system. Although the CPU implementation lags behind GPUs in raw throughput, the results demonstrate the feasibility of scaling generative model training on HPC-oriented CPUs and provide practical insights into architecture-specific optimization.

5.7 Scalability

We evaluate scalability under inter-node data parallelism from 1 to 256 nodes. Metrics include average runtime per iteration, achieved FLOPS, and parallel efficiency.

For weak scaling, the batch size per node is fixed at 112 and the global batch size grows proportionally with the node count. As shown in Figure 10, both the GEMM-optimized and the further tuned configurations exhibit near-linear scaling across four DiT model sizes. Performance and parallel efficiency improve with model size due to higher compute density. On DiT-XL/2, the GEMM-optimized configuration reaches over 1 PFLOPS (FP32) with 90.6% parallel efficiency at 256 nodes with 1024 processes.

Two factors underpin this efficiency. First, the proposed CFTP strategy reduces the number of ranks and turns intra-die communication into shared-memory accesses, minimizing communication overhead. Second, offloading communication to dedicated cores prevents the compute cores from incurring context switches and synchronization caused by blocked communication. We also report the results for the further tuned configuration, which adds multi-core and memory hierarchy optimizations on top of the GEMM improvements. Due to machine-allocation constraints, these runs were conducted up to 128 nodes. Within this range, the tuned configuration consistently achieves the best performance, and its scalability trend aligns with other configurations.

For strong scaling, we fix the global batch size and vary the number of nodes. Guided by memory-capacity constraints, we select three global batch sizes—448, 3,072, and 16,384—and evaluate strong scaling separately for each configuration (up to 256 nodes). As shown in Figure 11, efficiency decreases as node count increases. This is primarily because strong scaling yields a lower compute-to-communication ratio. In addition, as more nodes are added, the per-node batch size shrinks, reducing GEMM kernel efficiency. While our

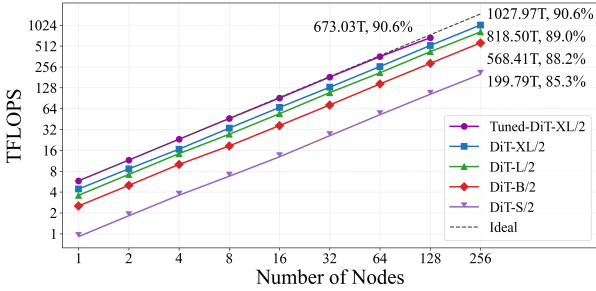


Figure 10. Weak scaling results for DiT training.

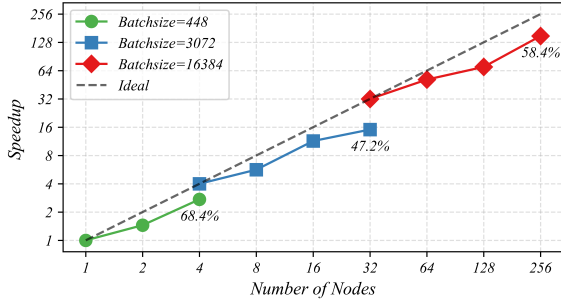


Figure 11. Strong scaling results for DiT-XL/2 training under varying batch sizes

optimizations effectively hide communication in the weak-scaling regime, under strong scaling the kernel-efficiency drop becomes the dominant factor.

6 Conclusion

This paper presents DiT-HC, an efficient and scalable training framework for Diffusion Transformers (DiT) on HPC-oriented CPU clusters. Through systematic optimization of operator implementations, parallelization strategies, and memory scheduling, DiT-HC is able to effectively leverage new hardware features such as matrix acceleration units and hierarchical memory architectures with on-package high-bandwidth memory. Experimental results show that DiT-HC delivers substantial improvements in end-to-end training performance and scalability. The framework achieves up to $8.2\times$ speedup over the native software stack, $87.7\times$ over OpenBLAS, and sustains more than 1 PFLOPS FP32 performance with 90.6% weak-scaling efficiency on 256 nodes. Its effectiveness is further confirmed on real-world remote sensing datasets, where it consistently achieves the best performance across tested configurations.

Beyond these results, DiT-HC demonstrates a viable path toward narrowing the gap between GPU-centric AI training and CPU-based supercomputing. As scientific computing increasingly integrates data-driven models with traditional simulations, DiT-HC offers a promising foundation for unifying AI and HPC workflows, with potential applications in data assimilation, climate modeling, and Earth system science. Future work will extend the framework to broader classes of generative models and explore deeper integration with domain-specific scientific applications.

References

- [1] [n. d.]. *oneAPI Deep Neural Network Library*. <https://github.com/ulxfoundation/oneDNN>
- [2] Guillermo Alaejos, Héctor Martínez, Adrián Castelló, Manuel F Dolz, Francisco D Igual, Pedro Alonso-Jordá, and Enrique S Quintana-Ortí. 2024. Automatic generation of ARM NEON micro-kernels for matrix multiplication. *The Journal of Supercomputing* 80, 10 (2024), 13873–13899.
- [3] Fan Bao, Shen Nie, Kaiwen Xue, Chongxuan Li, Shi Pu, Yaole Wang, Gang Yue, Yue Cao, Hang Su, and Jun Zhu. 2023. One transformer fits all distributions in multi-modal diffusion at scale. In *International Conference on Machine Learning*. PMLR, 1692–1717.
- [4] Annalisa Bracco, Julien Brajard, Henk A Dijkstra, Pedram Hassanzadeh, Christian Lessig, and Claire Monteleoni. 2025. Machine learning for the physics of climate. *Nature Reviews Physics* 7, 1 (2025), 6–20.
- [5] Mengxuan Chen, Haohuan Fu, Tao Zhang, and Lanning Wang. 2023. ResU-Deep: Improving the trigger function of deep convection in tropical regions with deep learning. *Journal of Advances in Modeling Earth Systems* 15, 11 (2023), e2022MS003521.
- [6] Runmin Dong, Shuai Yuan, Bin Luo, Mengxuan Chen, Jinxiao Zhang, Lixian Zhang, Weijia Li, Juepeng Zheng, and Haohuan Fu. 2024. Building bridges across spatial and temporal resolutions: Reference-based super-resolution via change priors and conditional diffusion model. In *Proceedings of the IEEE/CVF Conference on Computer Vision and Pattern Recognition*. 27684–27694.
- [7] Jack Dongarra. 2020. *Report on the Fujitsu Fugaku system*. Technical Report. Tech Report No ICL-UT-20-06, University of Tennessee, Innovative Computing
- [8] Xiaohui Duan, Yi Zhang, Kai Xu, Haohuan Fu, Bin Yang, Yiming Wang, Yilun Han, Siyuan Chen, Zhuangzhuang Zhou, Chenyu Wang, et al. 2025. An AI-Enhanced 1km-Resolution Seamless Global Weather and Climate Model to Achieve Year-Scale Simulation Speed using 34 Million Cores. In *Proceedings of the 30th ACM SIGPLAN Annual Symposium on Principles and Practice of Parallel Programming*. 524–538.
- [9] Jorge Ejarque, Rosa M Badia, Loïc Albertin, Giovanni Aloisio, Enrico Baglione, Yolanda Becerra, Stefan Boschert, Julian R Berlin, Alessandro D’Anca, Donatello Elia, et al. 2022. Enabling dynamic and intelligent workflows for HPC, data analytics, and AI convergence. *Future generation computer systems* 134 (2022), 414–429.
- [10] Patrick Esser, Sumith Kulal, Andreas Blattmann, Rahim Entezari, Jonas Müller, Harry Saini, Yam Levi, Dominik Lorenz, Axel Sauer, Frederic Boesel, et al. 2024. Scaling rectified flow transformers for high-resolution image synthesis. In *Forty-first international conference on machine learning*.
- [11] Haohuan Fu, Junfeng Liao, Jinzhe Yang, Lanning Wang, Zhenya Song, Xiaomeng Huang, Chao Yang, Wei Xue, Fangfang Liu, Fangli Qiao, et al. 2016. The Sunway TaihuLight supercomputer: system and applications. *Science China Information Sciences* 59 (2016), 1–16.
- [12] Xiao Fu, Weiling Yang, Dezun Dong, and Xing Su. 2024. Optimizing Attention by Exploiting Data Reuse on ARM Multi-core CPUs. In *Proceedings of the 38th ACM International Conference on Supercomputing*. 137–149.
- [13] William Gregory, Mitchell Bushuk, Yongfei Zhang, Alistair Adcroft, and Laure Zanna. 2024. Machine learning for online sea ice bias correction within global ice-ocean simulations. *Geophysical Research Letters* 51, 3 (2024), e2023GL106776.
- [14] Philipp Hess, Michael Aich, Baoxiang Pan, and Niklas Boers. 2025. Fast, scale-adaptive and uncertainty-aware downscaling of Earth system model fields with generative machine learning. *Nature Machine Intelligence* (2025), 1–11.
- [15] Jonathan Ho, Ajay Jain, and Pieter Abbeel. 2020. Denoising diffusion probabilistic models. *Advances in neural information processing systems* 33 (2020), 6840–6851.

[16] Langwen Huang, Lukas Gianinazzi, Yuejiang Yu, Peter D Dueben, and Torsten Hoefler. 2024. Diffda: a diffusion model for weather-scale data assimilation. *arXiv preprint arXiv:2401.05932* (2024).

[17] Yuzhen Huang, Xiaohan Wei, Xing Wang, Jiyan Yang, Bor-Yiing Su, Shivam Bharuka, Dhruv Choudhary, Zewei Jiang, Hai Zheng, and Jack Langman. 2021. Hierarchical training: Scaling deep recommendation models on large cpu clusters. In *Proceedings of the 27th ACM SIGKDD Conference on Knowledge Discovery & Data Mining*. 3050–3058.

[18] Jiazh Ji Jiang, Hongbin Zhang, Deyin Liu, Jiangsu Du, Xiaojiao Yao, Jinhui Wei, Pin Chen, Dan Huang, and Yutong Lu. 2024. Efficient Coupling Streaming AI and Ensemble Simulations on HPC Clusters. In *European Conference on Parallel Processing*. 313–328.

[19] Dhiraj Kalamkar, Evangelos Georganas, Sudarshan Srinivasan, Jianping Chen, Mikhail Shiryaev, and Alexander Heinecke. 2020. Optimizing deep learning recommender systems training on cpu cluster architectures. In *SC20: International Conference for High Performance Computing, Networking, Storage and Analysis*. IEEE, 1–15.

[20] Amirhossein Kazerouni, Ehsan Khodapanah Aghdam, Moein Heidari, Reza Azad, Mohsen Fayyaz, Ilker Hacihaliloglu, and Dorit Merhof. 2023. Diffusion models in medical imaging: A comprehensive survey. *Medical image analysis* 88 (2023), 102846.

[21] Ham Kim, YG Ham, YS Joo, and SW Son. 2021. Deep learning for bias correction of MJO prediction. *Nature Communications* 12, 1 (2021), 3087.

[22] Hyungyo Kim, Gaohan Ye, Nachuan Wang, Amir Yazdanbakhsh, and Nam Sung Kim. 2024. Exploiting intel® advanced matrix extensions (amx) for large language model inference. *IEEE Computer Architecture Letters* (2024).

[23] Benjamin Lefauze, Francisco Massa, Diana Liskovich, Wenhan Xiong, Vittorio Caggiano, Sean Naren, Min Xu, Jieru Hu, Marta Tin-tore, Susan Zhang, Patrick Labatut, Daniel Haziza, Luca Wehrstedt, Jeremy Reizenstein, and Grigory Sizov. 2022. xFormers: A modular and hackable Transformer modelling library. <https://github.com/facebookresearch/xformers>.

[24] Baolin Li, Rohin Arora, Siddharth Samsi, Tirthak Patel, William Arcand, David Bestor, Chansup Byun, Rohan Basu Roy, Bill Bergeron, John Holodnak, et al. 2022. Ai-enabling workloads on large-scale gpu-accelerated system: characterization, opportunities, and implications. In *2022 IEEE International Symposium on High-Performance Computer Architecture (HPCA)*. IEEE, 1224–1237.

[25] Liandeng Li, Jiarui Fang, Haohuan Fu, Jinlei Jiang, Wenlai Zhao, Conghui He, Xin You, and Guangwen Yang. 2018. swcaffe: A parallel framework for accelerating deep learning applications on sunway taihulight. In *2018 IEEE International Conference on Cluster Computing (CLUSTER)*. IEEE, 413–422.

[26] Cheng Lu, Yuhao Zhou, Fan Bao, Jianfei Chen, Chongxuan Li, and Jun Zhu. 2022. Dpm-solver: A fast ode solver for diffusion probabilistic model sampling in around 10 steps. *Advances in Neural Information Processing Systems* 35 (2022), 5775–5787.

[27] Alexander Quinn Nichol and Prafulla Dhariwal. 2021. Improved denoising diffusion probabilistic models. In *International conference on machine learning*. PMLR, 8162–8171.

[28] William Peebles and Saining Xie. 2022. Scalable Diffusion Models with Transformers. *arXiv preprint arXiv:2212.09748* (2022).

[29] Dustin Podell, Zion English, Kyle Lacey, Andreas Blattmann, Tim Dockhorn, Jonas Müller, Joe Penna, and Robin Rombach. 2023. Sdxl: Improving latent diffusion models for high-resolution image synthesis. *arXiv preprint arXiv:2307.01952* (2023).

[30] Ilan Price, Alvaro Sanchez-Gonzalez, Ferran Alet, Tom R Andersson, Andrew El-Kadi, Dominic Masters, Timo Ewalds, Jacklynn Stott, Shakir Mohamed, Peter Battaglia, et al. 2023. Gencast: Diffusion-based ensemble forecasting for medium-range weather. *arXiv preprint arXiv:2312.15796* (2023).

[31] Jeff Rasley, Samyam Rajbhandari, Olatunji Ruwase, and Yuxiong He. 2020. DeepSpeed: System optimizations enable training deep learning models with over 100 billion parameters. In *Proceedings of the 26th ACM SIGKDD international conference on knowledge discovery & data mining*. 3505–3506.

[32] Robin Rombach, Andreas Blattmann, and Björn Ommer. 2022. Text-guided synthesis of artistic images with retrieval-augmented diffusion models. *arXiv preprint arXiv:2207.13038* (2022).

[33] Mitsuhsisa Sato, Yutaka Ishikawa, Hirofumi Tomita, Yuetsu Kodama, Tetsuya Odajima, Miwako Tsuji, Hisashi Yashiro, Masaki Aoki, Naoyuki Shida, Ikuo Miyoshi, et al. 2020. Co-design for a64fx many-core processor and “fugaku”. In *SC20: International Conference for High Performance Computing, Networking, Storage and Analysis*. IEEE, 1–15.

[34] Mohammad Shoeybi, Mostofa Patwary, Raul Puri, Patrick LeGresley, Jared Casper, and Bryan Catanzaro. 2019. Megatron-lm: Training multi-billion parameter language models using model parallelism. *arXiv preprint arXiv:1909.08053* (2019).

[35] Cristina Silvano, Daniele Ielmini, Fabrizio Ferrandi, Leandro Fiorin, Serena Curzel, Luca Benini, Francesco Conti, Angelo Garofalo, Cristian Zambelli, Enrico Calore, et al. 2025. A survey on deep learning hardware accelerators for heterogeneous hpc platforms. *Comput. Surveys* 57, 11 (2025), 1–39.

[36] Jascha Sohl-Dickstein, Eric Weiss, Niru Maheswaranathan, and Surya Ganguli. 2015. Deep unsupervised learning using nonequilibrium thermodynamics. In *International conference on machine learning*. pmlr, 2256–2265.

[37] Yang Song, Jascha Sohl-Dickstein, Diederik P Kingma, Abhishek Kumar, Stefano Ermon, and Ben Poole. 2020. Score-based generative modeling through stochastic differential equations. *arXiv preprint arXiv:2011.13456* (2020).

[38] Maximilian Springenberg, Noelia Otero, Yuxin Xue, and Jackie Ma. 2025. DiffScale: Continuous Downscaling and Bias Correction of Subseasonal Wind Speed Forecasts using Diffusion Models. *arXiv preprint arXiv:2503.23893* (2025).

[39] Ye Tian, Zhen Jia, Ziyue Luo, Yida Wang, and Chuan Wu. 2024. DiffusionPipe: Training Large Diffusion Models with Efficient Pipelines. *Proceedings of Machine Learning and Systems* 6 (2024), 101–113.

[40] Cunyang Wei, Haipeng Jia, Yunquan Zhang, Kun Li, and Luhan Wang. 2022. LBBGEMM: A Load-balanced Batch GEMM Framework on ARM CPU s. In *2022 IEEE 24th Int Conf on High Performance Computing & Communications; 8th Int Conf on Data Science & Systems; 20th Int Conf on Smart City; 8th Int Conf on Dependability in Sensor, Cloud & Big Data Systems & Application (HPCC/DSS/SmartCity/DependSys)*. IEEE, 59–66.

[41] Martin Weidmann. 2021. Introducing the scalable matrix extension for the armv9-a architecture.

[42] Du Wu, Jintao Meng, Wenxi Zhu, Minwen Deng, Xiao Wang, Tao Luo, Mohamed Wahib, and Yanjie Wei. 2024. autoGEMM: Pushing the Limits of Irregular Matrix Multiplication on Arm Architectures. In *SC24: International Conference for High Performance Computing, Networking, Storage and Analysis*. IEEE, 1–15.

[43] Xiaoze Xu, Xiuyu Sun, Wei Han, Xiaohui Zhong, Lei Chen, Zhiqiu Gao, and Hao Li. 2025. Fuxi-da: A generalized deep learning data assimilation framework for assimilating satellite observations. *npj Climate and Atmospheric Science* 8, 1 (2025), 156.

[44] Yang You, Zhao Zhang, Cho-Jui Hsieh, James Demmel, and Kurt Keutzer. 2018. Imagenet training in minutes. In *Proceedings of the 47th international conference on parallel processing*. 1–10.

[45] Jinhui Yuan, Xinqi Li, Cheng Cheng, Juncheng Liu, Ran Guo, Shenghang Cai, Chi Yao, Fei Yang, Xiaodong Yi, Chuan Wu, et al. 2021. Oneflow: Redesign the distributed deep learning framework from scratch. *arXiv preprint arXiv:2110.15032* (2021).